Supplementary tables and figures

Table S1. SCC and RMSE of meridional wind at 850 hPa (units: m s^{-1}) between each pre-industrial experiment and observation within the region of 20–45°N and 105–135°E. The SCCs that are negative or confidence level below 95% are in bold.

Model	EASW		EAWW	
	SCC	RMSE	SCC	RMSE
CAM3.1	**–0.23**	1.67	0.85	1.05
HadAM3	0.73	0.74	0.94	0.74
LMDZ5A	0.60	1.01	0.73	1.47
MIROC4m-AGCM	0.49	1.41	0.82	1.16
MRI-CGCM2.3-AGCM	**–0.64**	1.79	0.86	1.04
CAM4	0.52	1.25	0.80	1.30
ECHAM5	**–0.01**	1.28	0.92	1.02
ModelE2-R	0.80	0.71	0.90	0.86
CCSM4	0.48	1.14	0.76	1.42
HadCM3	0.76	0.94	0.93	0.72
IPSLCM5A	0.64	1.04	0.84	1.18
MIROC4m	0.56	1.37	0.72	1.47
MRI-CGCM2.3	0.53	0.89	0.93	0.78
NorESM-L	0.80	1.50	0.75	1.53
COSMOS	**0.15**	1.23	0.94	0.81

Table S2. SCC and RMSE of SAT (units: °C) and precipitation (units: mm/day) between each pre-industrial experiment and observation within China.

Model	Annual				Summer				Winter			
	TAS		Precipitation		TAS		Precipitation		TAS		Precipitation	
	SCC	RMSE	SCC	RMSE	SCC	RMSE	SCC	RMSE	SCC	RMSE	SCC	RMSE
CAM3.1	0.97	1.94	0.61	1.10	0.95	2.35	0.73	1.73	0.98	2.31	0.40	0.65
HadAM3	0.99	1.16	0.91	0.70	0.97	1.56	0.90	1.41	0.98	2.11	0.77	0.52
LMDZ5A	0.98	2.24	0.81	0.82	0.98	1.89	0.84	1.45	0.96	2.98	0.59	0.60
MIROC4m-AGCM	0.97	2.36	0.68	1.06	0.94	2.44	0.60	2.40	0.97	2.72	0.63	0.52
MRI-CGCM2.3-AGCM	0.96	2.19	0.54	1.39	0.92	2.56	0.61	2.33	0.98	2.46	0.72	0.70
CAM4	0.94	2.66	0.57	1.28	0.91	2.93	0.48	2.54	0.96	2.86	0.34	0.83
ECHAM5	0.94	2.75	0.82	1.14	0.88	3.19	0.79	2.42	0.96	3.04	0.82	0.54
ModelE2-R	0.94	3.18	0.62	2.23	0.95	2.80	0.55	4.13	0.92	4.47	0.67	1.02
CCSM4	0.97	1.91	0.76	1.07	0.97	1.82	0.73	2.18	0.97	2.68	0.80	0.41
HadCM3	0.99	1.27	0.90	0.68	0.99	0.94	0.87	1.40	0.98	2.25	0.81	0.44
IPSLCM5A	0.98	2.36	0.82	0.79	0.98	2.12	0.84	1.34	0.96	2.99	0.55	0.69
MIROC4m	0.96	2.55	0.78	0.88	0.93	2.67	0.68	1.95	0.97	2.95	0.67	0.56
MRI-CGCM2.3	0.96	2.24	0.69	1.11	0.92	2.64	0.68	2.06	0.98	2.31	0.76	0.68
NorESM-L	0.93	2.79	0.71	1.10	0.89	3.16	0.62	2.20	0.96	3.07	0.59	0.62
COSMOS	0.94	2.75	0.82	0.98	0.87	3.25	0.83	1.64	0.96	2.97	0.69	0.77

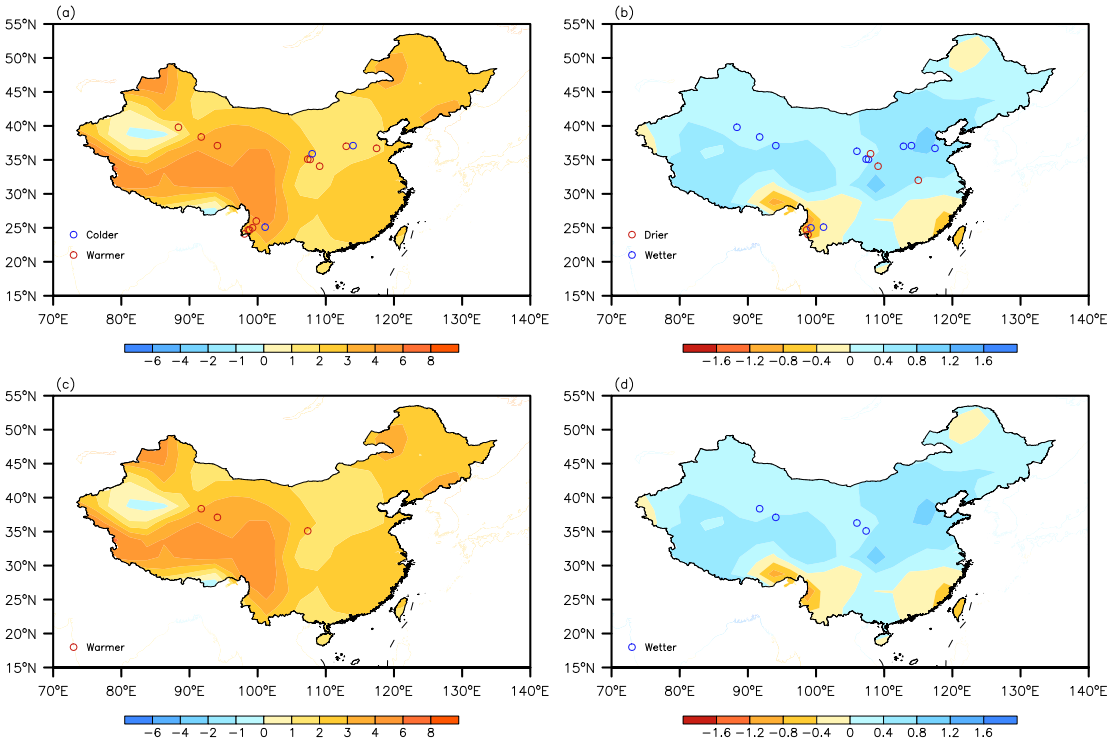

Fig. S1. The reconstructed temperature and humidity changes in mid-Pliocene compared to late Quaternary on the basis of proxy data listed in Table 2. (a) and (b) show all reconstructed data, (c) and (d) show reconstructed data with high reliability for age control and climate interpretation. The shaded value is the MMM for annual SAT and precipitation changes shown in Fig 4a and 4b.

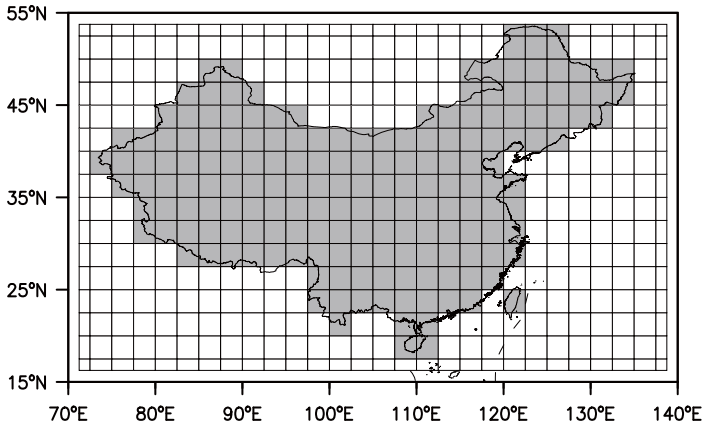

Fig. S2. Shaded grids used to analyze the model results in China.

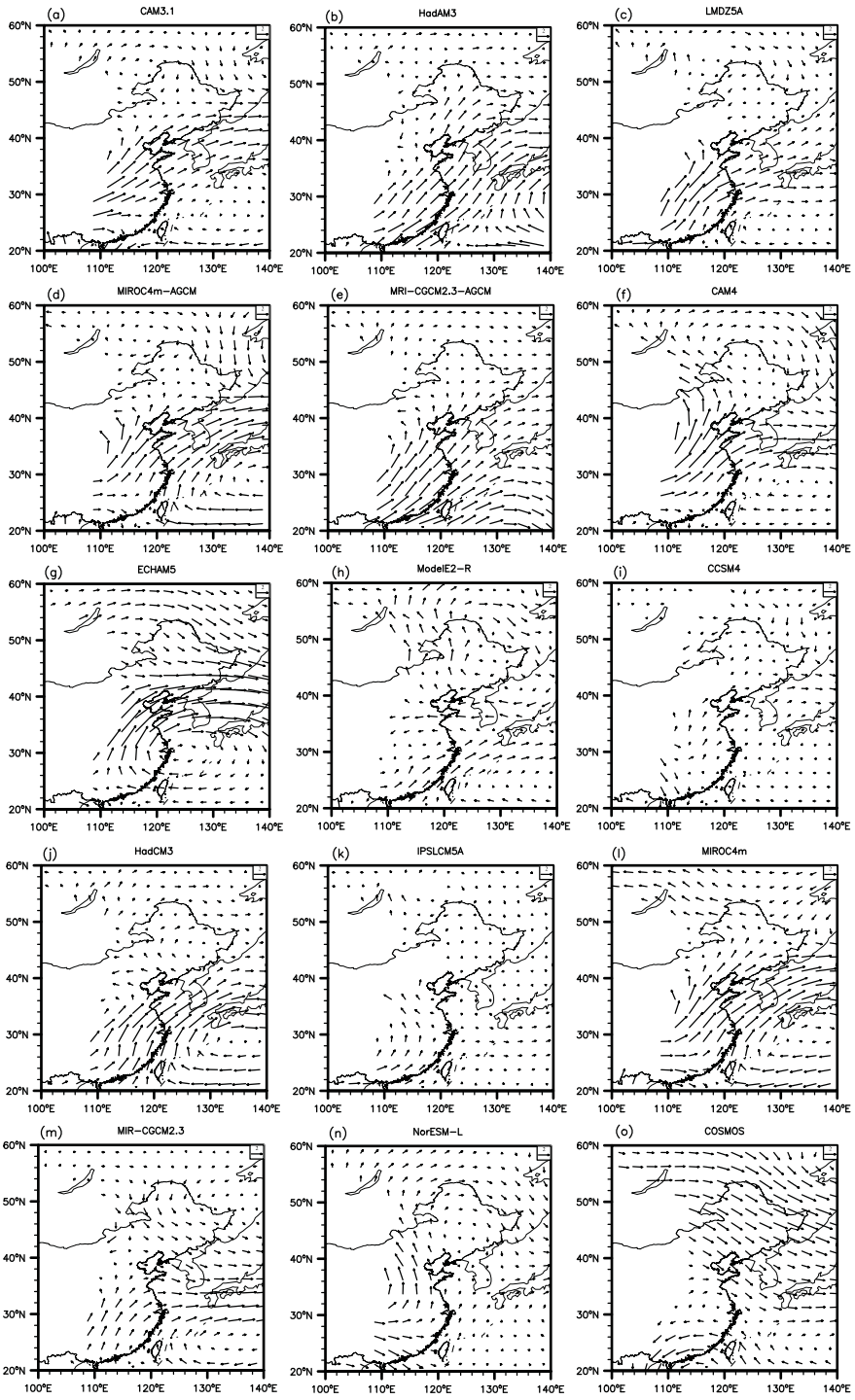

Fig. S3. The differences of summer monsoon winds (units: m s^{-1}) between mid-Pliocene and pre-industrial experiments. Regions with an elevation above 1500m are left blank.

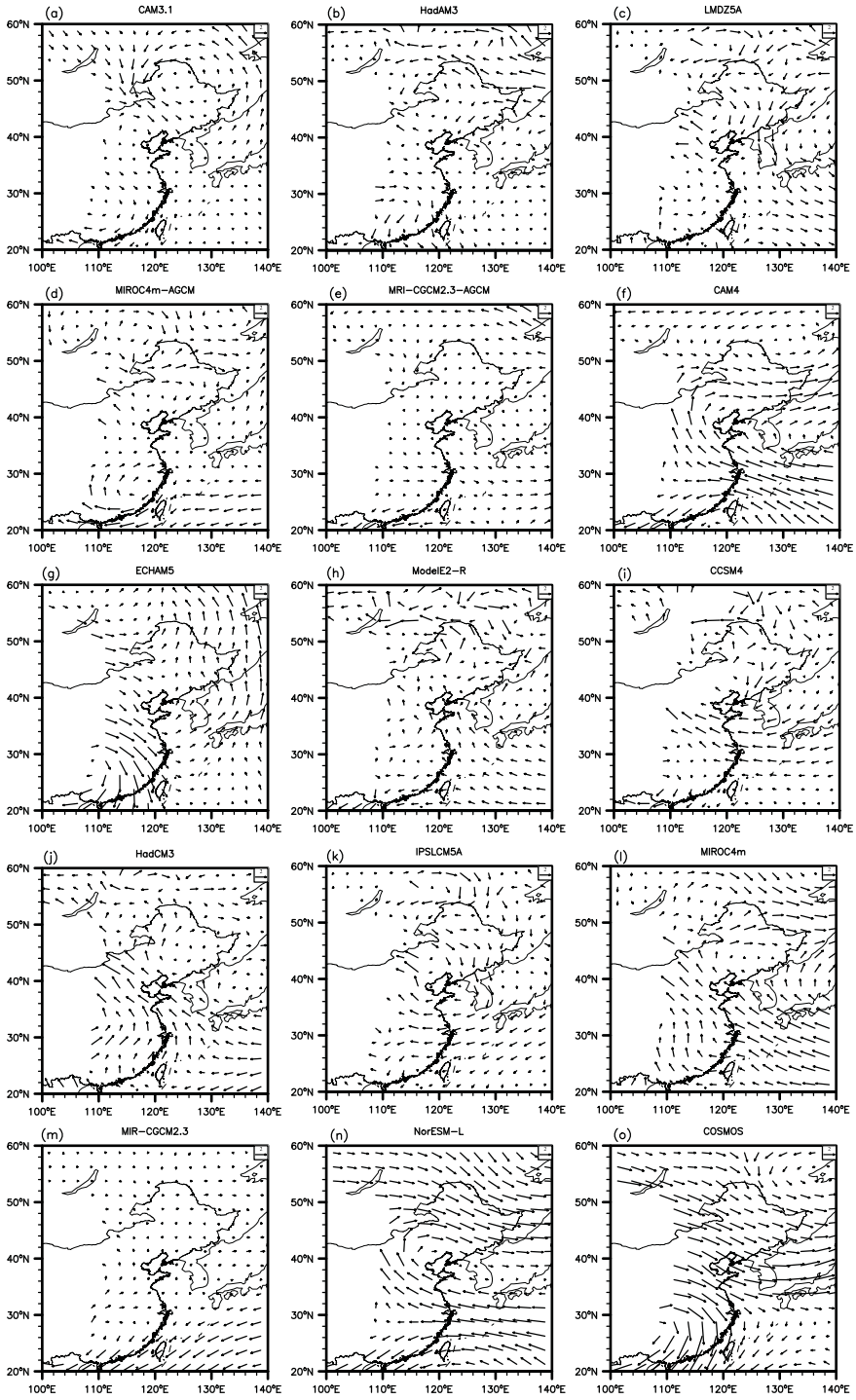

Fig. S4. Same as Fig. S3, but for the differences of winter monsoon winds (units: m s^{-1}).

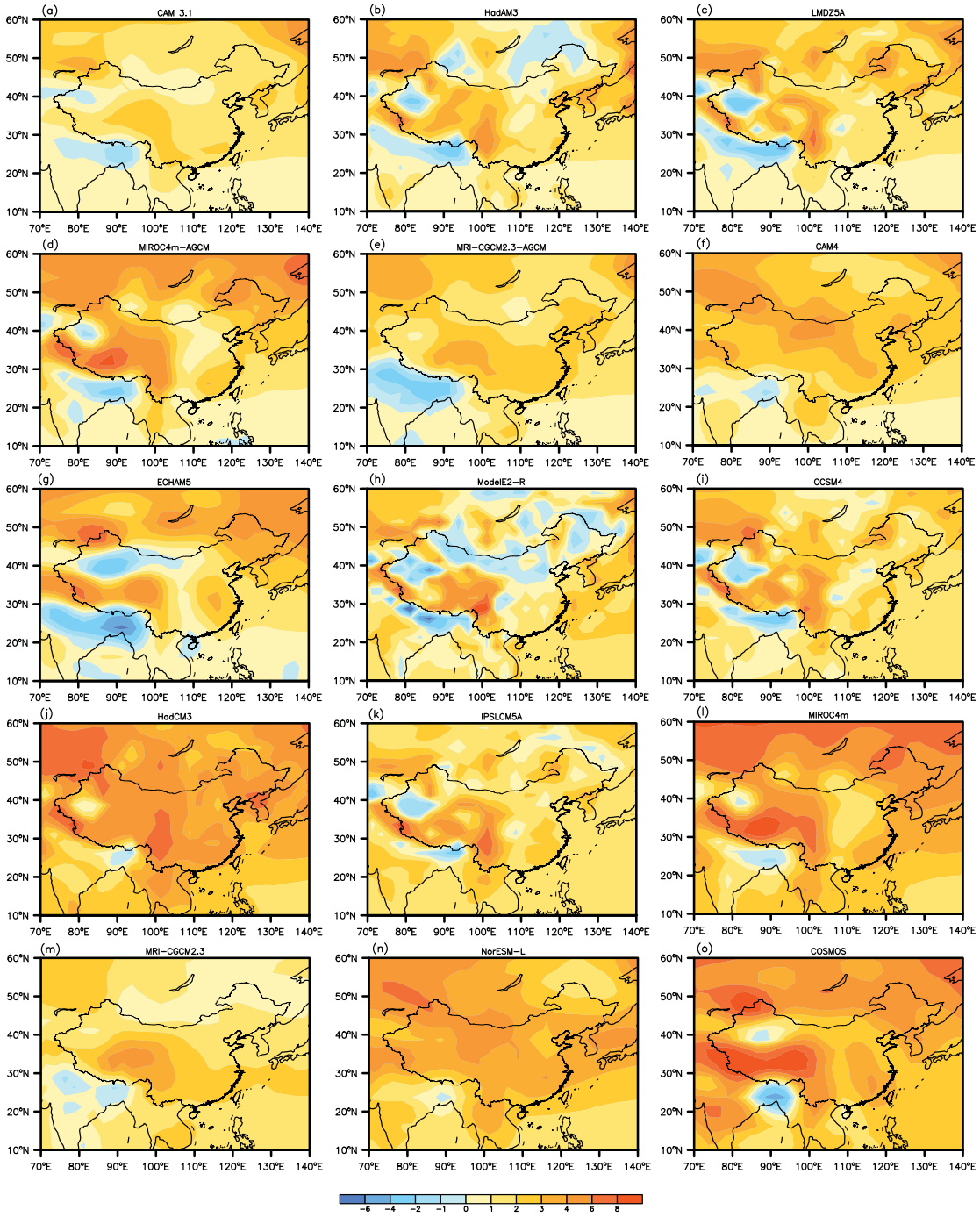

Fig. S5. Annual mean SAT differences (units: °C) between mid-Pliocene and pre-industrial experiments.

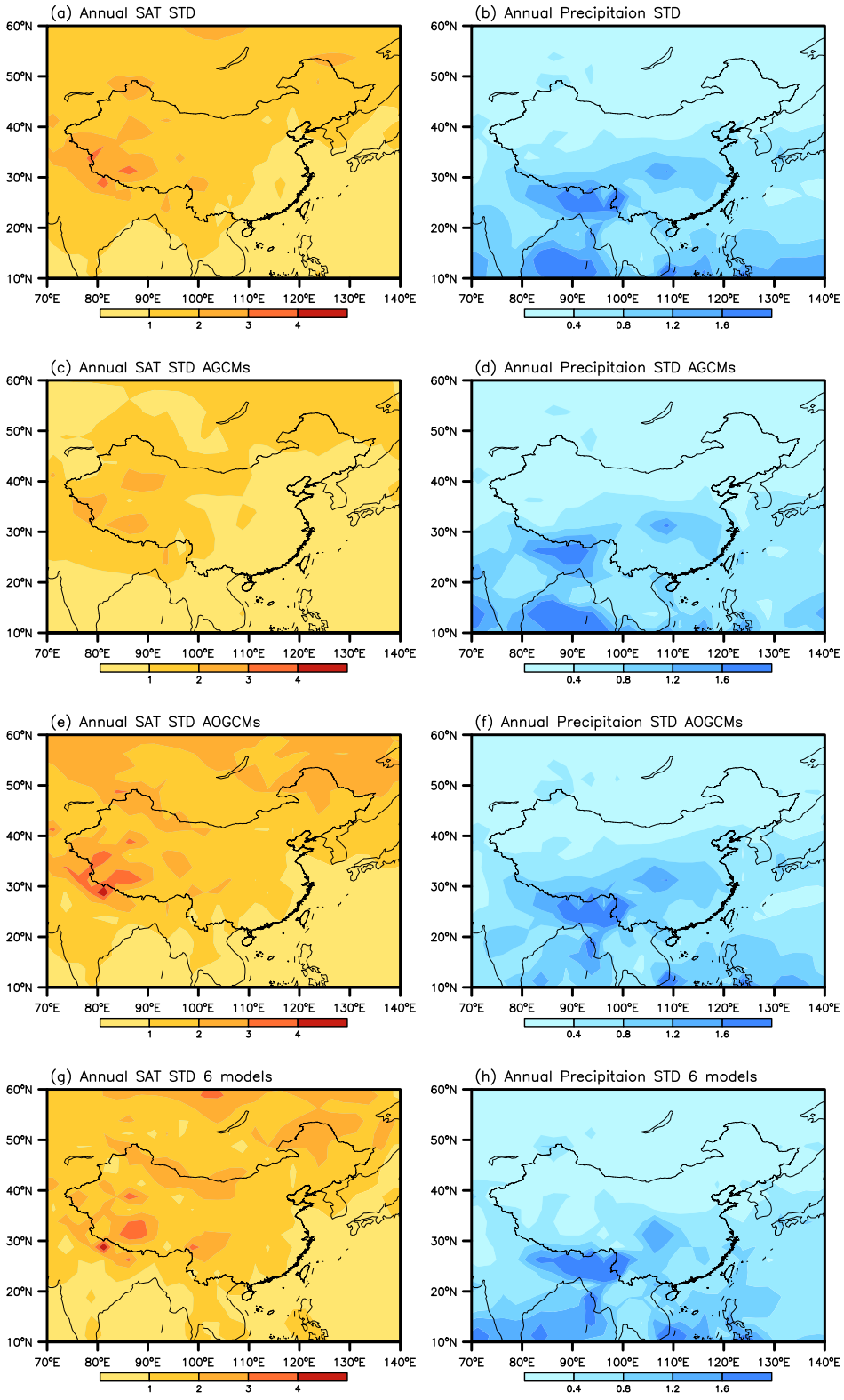

Fig. S6. The standard deviation of the simulated differences in annual SAT (left column, units: °C) and precipitation (right column, units: mm/day) between mid-Pliocene and pre-industrial experiments. (a) and (b) are of all models, (c) and (d) are for AGCMs, (e) and (f) are for AOGCMs, (g) and (h) are of the six models that simulate weakened EAWW listed in table 3.

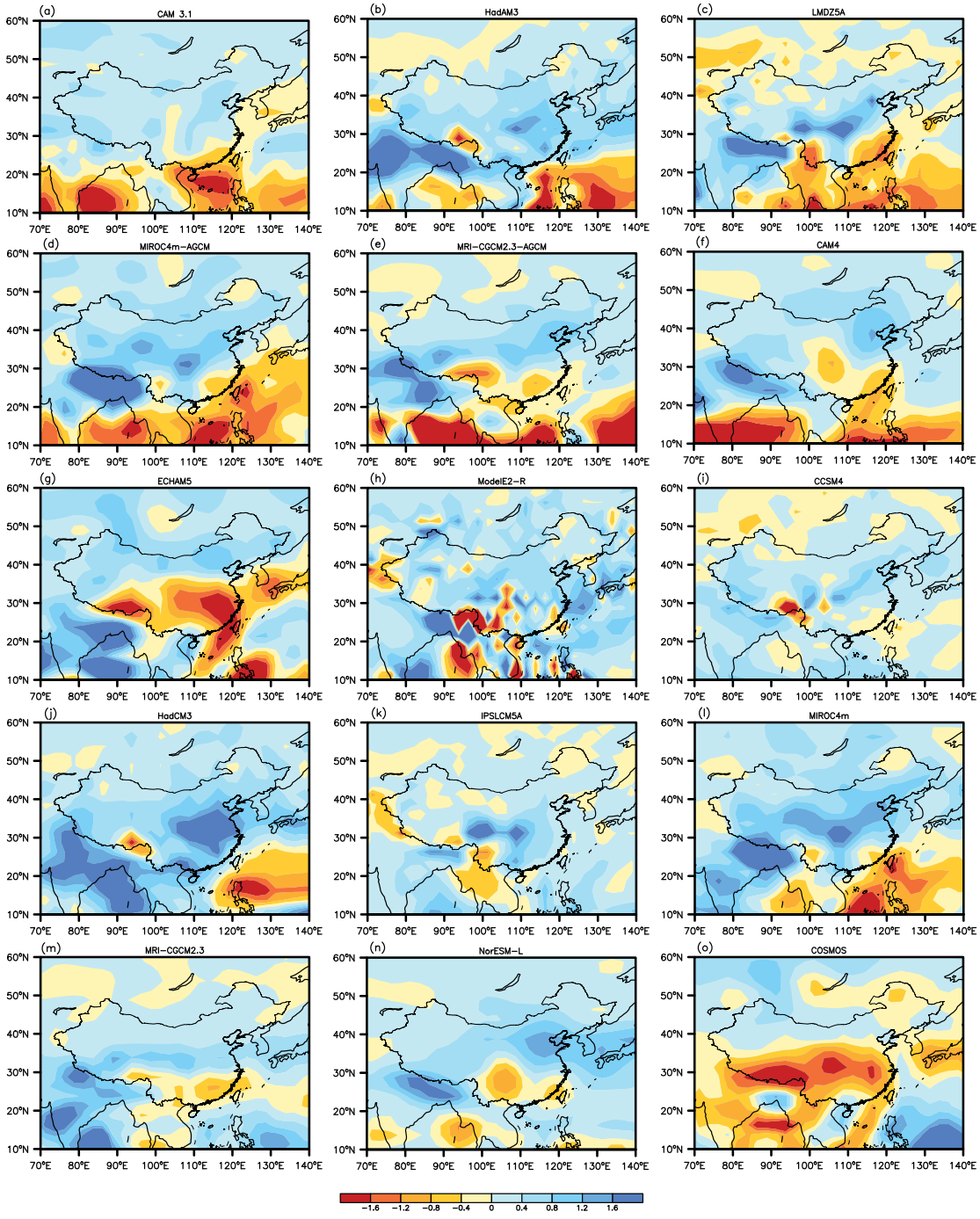

Fig. S7. Same as Fig. S5, but for the differences of the annual mean precipitation (units: mm/day).

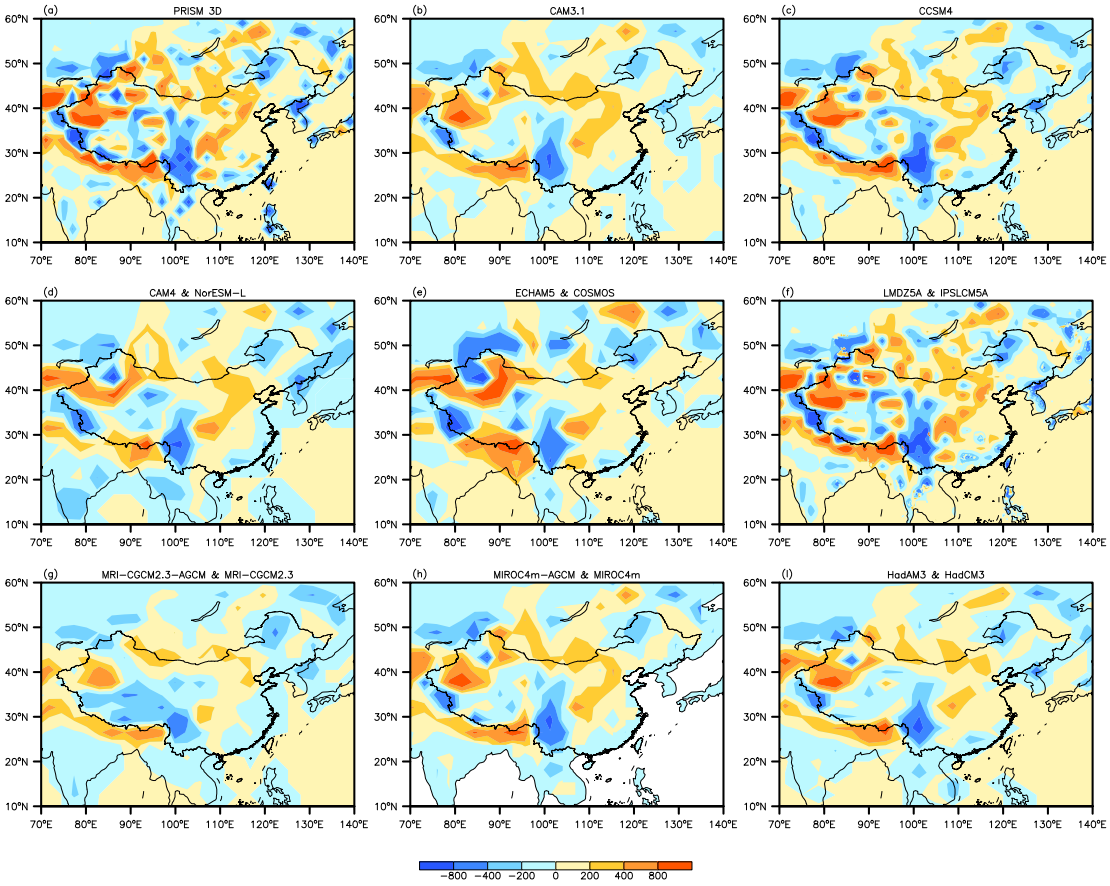

Fig. S8. Topography differences (units: m) between mid-Pliocene and pre-industrial experiments provided in PRISM3D or used by different models.